J Mol Model (2013) 19:2343–2353
DOI 10.1007/s00894-013-1781-4

ORIGINAL PAPER

Stabilization of gold nanowires inside nanoaggregates of cyclo[8]thiophene, cyclo[8]selenophene, and cyclo[8]tellurophene: a theoretical study

Xiaomin Huang · Serguei Fomine

Received: 27 November 2012 / Accepted: 21 January 2013 / Published online: 9 February 2013

Abstract The stabilities and electronic properties of gold clusters containing up to six atoms trapped inside cyclo[8]thiophene (CS8), cyclo[8]selenophene (CSe8), and cyclo[8]tellurophene (CTe8) nanoaggregates have been studied using the M06 functional. The 6-31G(d) basis set was used for all atoms except Au and Te, for which the LANL2DZ(d,p) pseudopotential basis set was applied. Single-point energy calculations were performed with the 6-311G(d,p) basis set for all atoms except for Au and Te, for which the cc-TZVP-pp pseudopotential basis set was used. Among the three studied macrocycles, only CS8 and CSe8 were found to be capable of nanoaggregate formation. In the lowest-energy conformer of CTe8, the tellurophene fragments adopt an *anti* orientation, thus impeding a tubular arrangement of the macrocycles. The formation of gold clusters inside the CS8 and CSe8 nanoaggregates is a thermodynamically favorable process, and could represent a potentially useful method of stabilizing metal nanowires. The binding energy between the nanoaggregate and the gold cluster is always higher for selenium-containing complexes than for sulfur-containing ones because Se has a higher affinity than S for Au in such complexes. Interactions of the gold cluster with the nanoaggregate walls can change the geometry of the most stable isomer for the cluster. The relative energies of different isomers are rather similar, suggesting that they coexist. For nanoaggregates containing Au_6 clusters, the cluster geometry when it is inside a nanoaggregate is different from the geometry of the cluster when it is not inside the nanoaggregate, due to the geometric restrictions imposed by the nanoaggregate cavity. The reorganization energy needed to change the geometry leads to lower binding energies for these complexes compared to those of some smaller systems, although the formation of a complex between Au_6 and a nanoaggregate with six CS8 or CSe8 macrocycles is still thermodynamically viable.

Keywords Nanowire · Nanotube · Polythiophene · Polyselenophene · Gold cluster

X. Huang · S. Fomine (✉)
Instituto de Investigaciones en Materiales, Universidad Nacional Autónoma de México, Apartado Postal 70-360, CU, Coyoacán, DF CP 04510, México
e-mail: fomine@servidor.unam.mx

Introduction

Molecular electronics has recently been recognized to be one of the most viable options for creating nanoscale electronic devices [1–4]. A great variety of potentially useful molecular electronic devices, such as molecular rectifiers, resonant tunneling diodes, wires, and storage devices have been designed and studied both experimentally and theoretically [5–10]. Nanotubes (NTs) and nanowires (NWs) are among the two most important groups of so-called quasi one-dimensional nanostructures. They are considered potential materials for nanoelectronics, photocatalytic nanolithography, microscopy, and other modern nanotechnological fields. Finite-size effects cause dramatic changes in the structural, electronic, magnetic, and optical properties of these nanoscale materials compared to those of bulk materials. However, free-standing NWs become less stable as they get thinner [11]. Therefore, to ensure the practical applicability of NWs, it is extremely important to enhance their structural stability. One method of stabilizing an NW that has been studied both experimentally and theoretically is to fill the interior of a carbon NT with the NW [12–15]. Thus, over the past few years, nanocomposites based on NTs and NWs have been fabricated, and these have shown some enhanced properties [16–19]. For instance, carbon NTs filled with metals such as Cr [20], Fe, [13], Co [21],

Ni [22], Cu [23], and Ge [24] have been prepared. A variety of methods have been used to fill the NTs, including arc discharge, chemical vapor deposition, and laser vaporization. When the metal has a low melting point, as seen for Pb and Bi, encapsulation is usually achieved by placing open-capped NTs in the liquid phase and allowing the atoms to enter the NT cavity [12]. However, all of these methods that involve filling NTs with metal atoms are rather laborious, and lead to defects and incomplete filling. These shortcomings might be avoided if the NT and NW were to be formed simultaneously. It has recently been demonstrated that cyclooligothiophenes (CTs) are able to form stable columnar nanoaggregates due to π–π stacking interactions between CT macrocycles [25]. The binding energy between macrocycles is >40 kcal mol^{-1}. These macrocycles should be able to form inclusion complexes with metal ions when the ion matches the size of the macrocycle cavity. Late transition metals are the best candidates to form inclusion complexes with CT macrocycles, due to their excellent affinity for sulfur. Reducing the metallic ions, which is a relatively easy process for late transition metals, leads to the formation of a neutral inclusion complex that is able to self-assemble to form an NW inside the NT. This process is depicted schematically in Fig. 1. It has recently been demonstrated that the formation of NWs of gold and silver inside nanoaggregates consisting of CTs is thermodynamically favorable and could potentially be a useful method of stabilizing metal NWs [26]. The formation of metal inclusion complexes significantly increases the binding energy between the macrocycles and changes the geometry of the NW compared to that seen for the metal-free clusters, due to the size restriction imposed by the nanoaggregate cavity.

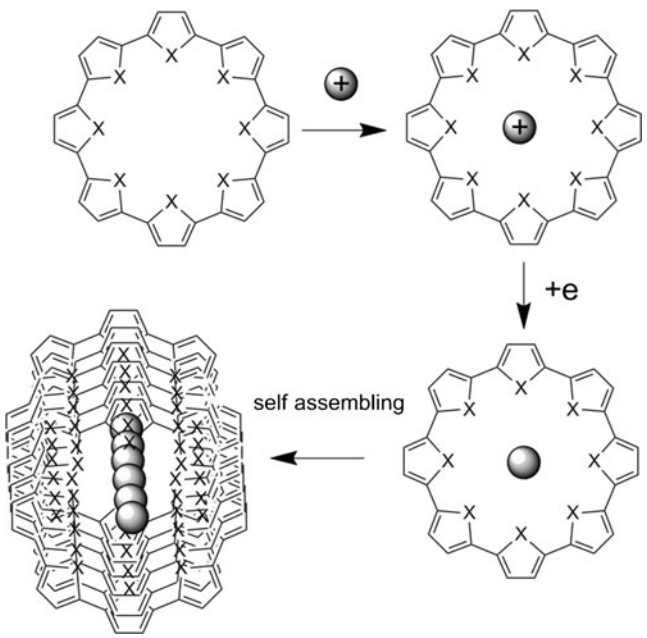

Fig. 1 Formation of a metallic nanowire inside a nanoaggregate

Together with sulfur, selenium and tellurium belong to the chalcogen group of elements, and have similar chemical properties. Thus, Se and Te form seleno- and tellurophenes, respectively, which are similar to thiophenes and can be polymerized to polyselenophene (PSe) and polytellurophene (PTe) [27]. PTe is a rather unstable black powder under normal conditions, with a predicted band gap of 1.87 V [28], whereas PSe is stable under normal conditions and its band gap is very similar to that of PTh—about 2 eV [27]—although theoretical calculations predict a slightly lower value of 1.86 eV [29]. However, there are no known cyclic oligomers of PSe and PTe that are analogous to cyclic oligothiophenes [30]. Therefore, the goal of the research described in the present paper was to predict the most important electronic properties of cyclic oligoselenophenes and oligotellurophenes, explore their ability to form nanoaggregates, evaluate the possibility of forming gold nanowires inside such nanoaggregates, and compare their properties with those of cyclic oligothiophenes.

Computational details

All calculations were carried out using the Gaussian 09 suite of programs [31]. The M06 functional [32] was used for geometry optimization, in combination with the 6-31 G(d) basis set for H, C, S, and Se atoms and the LANL2DZ(d,p) pseudopotential basis set for Te and Au. No symmetry restrictions were imposed during the optimizations. The same basis sets were used in combination with the time-dependent implementation of the CAM-B3LYP functional [33] to estimate the lowest excitation energies of the nanoaggregates. The M06 functional has already been shown to produce excellent results for weakly bound and transition metal complexes. The M06/LANL2DZ model predicts the interatomic distance in the Au_2 molecule to within 0.05 Å of the actual value [34]. To refine the energy, single-point energy calculations were carried out using the larger cc-TZVP-pp pseudopotential basis set for Au and Te and the 6-311 G(d,p) basis set for the other atoms. Tubular aggregates of macrocycles and their NW inclusion complexes were denoted nCS8 and nCS8-Au, respectively, for cyclooligothiophene; nCSe8 and nCSe8-Au, respectively, for cyclooligoselenophene; and nCTe8 and nCTe8-Au, respectively, for cyclooligotellurophene, where "n" is the number of macrocyclic units in the aggregate and "-Au" indicates that the macrocyclic aggregate has n Au atoms in its cavity. The geometries of the lowest-energy structures for the Au clusters, which were used to calculate the

binding energies, were obtained from [35, 36]. Overlap population density-of-states plots were obtained using the AOMix software package [37, 38].

Results and discussion

For the cyclooligothiophenes, the *syn* conformation is the most stable one for macrocycles that contain less than 20 repeating units. For larger macrocycles, the most stable conformation is *anti*, similar to what is seen for linear oligothiophenes [39]. Thus, the energy difference between the *syn* and *anti* conformations of CS8 was calculated to be 11.0 kcal mol^{-1}. The calculations revealed that cycloselenophene (CSe8) follows the same trend, but the difference between the *syn* and *anti* conformations decreases to 3.3 kcal mol^{-1} due to the larger atomic radius of Se compared to S. The situation changes for the CTe8 macrocycle. The *anti* conformation becomes 8.9 kcal mol^{-1} less stable than the corresponding *syn* conformation of CTe8 due to increased steric hindrance in the *syn* conformation. Therefore, only CS8 and CSe8 are capable of forming columnar nanoaggregates; CTe8 is unable to form such structures. For this reason, we only studied the complexes of a single CTe8 macrocycle with an Au atom.

Table 1 shows the binding energies and the most important geometric parameters for the nCS8 and nCSe8 nanoaggregates. Using a larger basis set for both geometry optimization and binding-energy evaluations results in an increase in the average binding energy for nCS8 nanoaggregates compared to that obtained at the lower level of theory employed in previous paper [26], from 28–29 to 42–43 kcal mol^{-1}. It is worth noting that the simpler M06/3–21 G(d) model produced binding energies of 42–44 kcal mol^{-1}, close to the values obtained with larger basis set, M06/6–311 G(d,p)//M06/6–31 G(d), which is probably due to two errors—the underbinding and the basis set superposition error—canceling each other out. As was seen for nCS8 nanoaggregates, the binding energies of nCSe are very similar for nanoaggregates of different sizes: 37–38 kcal mol^{-1} (Table 1). These values are somewhat lower than those for the nCS8 nanoaggregates. Since macrocycles mostly interact with each other via dispersion, the increase in the binding energy seen for nCSe8 compared to nCS8 would be expected due to the higher polarizability of the Se atom compared to the S atom. However, the interaction of the 2*p* orbitals of carbon with the 4*p* orbitals of Se is less efficient than that between the 2*p* orbitals of carbon and the 3*p* orbitals of Se, leading to a more localized lone pair on the Se atom. This difference is evident when comparing the inter-ring bond lengths in linear oligothiophenes and oligoselenophenes. These bond lengths are slightly larger in oligothiophenes (1.437 vs. 1.432 Å for the central bond of the octamer), revealing that oligoselenophene has a higher contribution from the quinoid structure and thus a more localized lone pair on the Se atom. This trend is maintained for oligotellurophene, where the inter-ring central bond is even shorter (1.430 Å). The dihedral angles (S–C–C–S and Se–C–C–Se, respectively) are larger for nCSe8 than for nCS8 due to stronger steric hindrance between the Se atoms than between the S atoms (Table 1). These angles are smallest for the individual macrocycles and increase for nanoaggregates (both nCS8 and nCSe8). The increased dihedral angle allows for closer contacts in the nanoaggregate, thus enhancing the interaction energy. As seen in Table 1, the larger dihedral angles in nCSe8 nanoaggregates (39°) than in nCS8 aggregates (33–34°) result in smaller interplane distances for the former.

Table 1 Binding energies (E_b, kcal mol^{-1}), interplane distances (D, Å), dihedral angles, and lowest excitation energies (S0→S1, eV) of nCS8, nCSe8, and nCTe8 nanoaggregates

Molecule	E_b	D	Dihedral angle (°)	S0→S1
CS8	–	–	13.6	2.83
CSe8	–	–	34.1	2.83
CTe8	–	–	113.3	2.49
2CS8	42.8	3.47	33.0	3.01
2CSe8	37.5	3.38	39.5	3.09
3CS8	42.5	3.44	34.3–35.2	3.04
3CSe8	38.0	3.42	39.4–40.6	3.14
4CS8	42.4	3.47	33.8–35.5	3.03
4CSe8	37.9	3.41	39.1–40.4	3.13
6CS8	42.2	3.42	34.2–35.6	3.04
6CSe8	37.8	3.38	39.8–40.3	3.15

The lowest excitation energies for the nanoaggregates and their corresponding macrocycles are listed in Table 1. For all three macrocycles, the most important contribution to the lowest excitation energy is HOMO–LUMO excitation. While the HOMO consists mostly of carbon 2p_z orbitals, the LUMO receives an important contribution from the p_z orbital of the heteroatom. As seen in Table 1, the lowest-energy transitions for CS8 and CSe8 are similar, while the lowest-energy transition for CTe8 is redshifted. These results are in line with known experimental data for PTh and PSe, as very similar band gaps are observed for these two polymers [27]. Calculations, however, predict a slightly smaller band gap for PSe [29] when planar structures are assumed. This phenomenon is related to the fact that heterocycle aromaticity decreases from thiophene to tellurophene, so the contribution from the quinoid structure in the polymer increases in the same order, leading to a decrease in the band gap. However, the twist angle in CSe8 is larger than that in CS8, which increases the band gap for CSe8. Therefore, the similar lowest excitation energies of CS8 and

CSe8 are the result of two opposite trends. In the case of CTe8, the most important factor is the increase in the contribution of the quinoid structure, which leads to a noticeable decrease in the lowest excitation energy.

The lowest excitation energies for the nanoaggregates are higher than those of their corresponding macrocycles for both nCS8 and nCSe8 and are practically independent of n (although they are slightly higher for nCSe8; see Table 1). The higher excitation energies of the nanoaggregates are related to the larger twist angles between the rings in the nanoaggregates compared to those in the individual macrocycles, while the lack of a dependence of the excitation energy on the nanoaggregate size is an indication of that the macrocycles in nanoaggregates are optically isolated, and that excitations of individual macrocycles take place. Taking into account this fact, it is easy to estimate the optical band gap for infinitely large nanoaggregates of nCS8 and nCSe8: 3.0 and 3.15 eV, respectively.

The most important properties of the nCS8-Au, nCSe8-Au, and nCTe8-Au nanoaggregates are listed in Table 2. It was shown previously [26] that the formation of a gold NW inside an nCS8 nanoaggregate is a thermodynamically favorable process.

CS8-Au, CSe8-Au, and CTe8-Au

The binding energies (E_b) of individual macrocycles with metal atoms increase from CS8-Au to CTe8-Au. Each complex has a different lowest-energy conformation. In the lowest-energy conformation of CS8-Au, the Au atom is positioned in the center of the macrocycle cavity, while the metal atom is at the macrocycle wall in the lowest-energy conformations of CSe8-Au and CTe8-Au (Fig. 2).

The energy difference between the symmetric conformation of CSe8-Au (which is similar to that of CS8-Au) and the lowest-energy asymmetric one is 1.3 kcal mol^{-1}. This difference is related to the stronger affinity of Au atoms for Se and (especially) Te compared to S. While the shortest distance between Au and S in C8S-Au is 3.72 Å, which is larger than the sum of their VDW radii, this distance is 2.91 and 2.89 Å, respectively, in C8Se-Au and C8Te-Au, which is less than the sum of their respective VDW radii. Therefore, the interaction between Au and S is mostly VDW in nature, while there is actual chemical bond formation between Au and Se or Te. The overlap population density-of-states (OPDOS) of the metal-containing aggregates are shown in Fig. 3. The positive regions correspond to the bonding and the negative to the antibonding levels between the fragments (the nanoaggregate and the Au cluster). When the plots for C8S-Au, C8Se-Au, and C8Te-Au are compared, it is clear that the strongly antibonding levels at 6 eV are completely full, while the antibonding levels at 5 and 4.4 eV for C8Se-Au and C8Te-Au, respectively, are only half full, explaining the higher binding energies of the C8Se-Au and C8Te-Au complexes compared to that of the C8S-Au complex. On the other hand, the stronger bonding character of the MOs between −12 and −8 eV explains the higher binding energy of C8Te-Au than C8Se-Au. The antibonding levels in C8S-Au are almost pure MOs of CS8, while those in C8Se-Au and C8Te-Au receive contributions from both macrocycle and cluster orbitals. Although the NBO charge on the Au atom is very similar for C8S-Au and C8Se-Au (slightly negative in both cases), the charge transfer is significantly higher for C8Te-Au (Table 2) due to the lower electronegativity of Te than S and Se.

Table 2 Binding energies between Au clusters and nanoaggregates (E_b, kcal/mol^{-1}), interplane distances (D, Å), dihedral angles, and natural charges on Au clusters in nCS8-Au, nCSe8-Au, and nCTe8-Au complexes. The *values in parentheses* are per atom

Complex	E_b	D	Dihedral angle (°)	Charge
CS8-Au	11.0	–	28.7	−0.09
CSe8-Au	14.9	–	31.0	−0.07
CTe8-Au	27.6 (13.8)	–	103.0–118.6	−0.17
2CS8-Au	36.5 (18.2)	3.29	13.7–36.5	−0.51 (−0.21)
2CSe8-Au	41.0 (13.7)	3.42	34.8–47.4	−0.73 (−0.37)
3CS8-Au	52.3 (17.4)	3.41	30.0–42.5	−0.89 (−0.30)
3CSe8-Au	62.4 (20.8)	3.41	37.6–49.1	−1.23 (−0.41)
4CS8-Au-R	66.7 (16.7)	3.46	31.8–47.5	−1.25 (−0.31)
4CSe8-Au-R	74.9 (18.7)	3.39	37.2–51.7	−1.73 (−0.43)
4CS8-Au-T	68.2 (17.0)	3.45	31.8–47.1	−1.22 (−0.30)
4CSe8-Au-T	74.4 (18.6)	3.39	37.2–51.3	−1.72(−0.43)
6CS8-Au-T	53.0 (8.8)	3.40	31.0–46.7	−1.90 (−0.32)
6CS8-Au-R	61.4 (10.2)	3.40	31.0–46.8	−1.88 (−0.31)
6CSe8-Au-T	59.5 (9.9)	3.37	37.3–49.1	−2.60 (−0.43)
6CSe8-Au-R	56.1 (9.4)	3.38	37.3–49.8	−2.51(−0.42)

2CS8-Au and 2CSe8-Au

Qualitatively, the geometries of these two complexes are very much alike. The gold Au_2 cluster is tilted with respect to the nanoaggregate axis (Fig. 4), maximizing its interactions with heteroatoms of the macrocycle. The shortest heteroatom to Au distance is 2.65 Å for C8S-Au and 2.76 Å for C8S-Se complex. The improved fit of Au_2 into the nanoaggregate cavity for 2CS8-Au and 2CSe8-Au as compared to CS8-Au and CSe8-Au, respectively, leads to a higher interaction energy between the cluster and the nanoaggregate. Thus, as seen in Table 2, the binding energy between the nanoaggregate

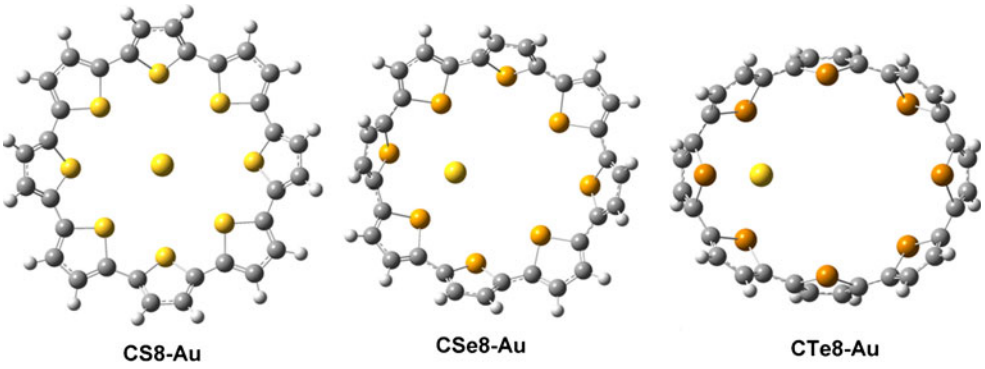

Fig. 2 Optimized geometries of the CS8-Au, CSe8-Au, and CTe8-Au complexes

and the Au cluster for 2CS8-Au or 2CSe8-Au is more than twice as high as that for CS8-Au or CSe8-Au, and a similar situation is observed for the natural charge. Following the trend, the binding energy is higher and the natural charge on the metal cluster is more negative for 2CSe8-Au than for 2CS8-Au (Table 2). It is worth noting that the Au–Au distance is the same for these two complexes, 2.61 Å. The adjustment of the nano-aggregate geometry to accommodate the Au_2 cluster leads to an increase in the dihedral angle between the thiophene and selenophene fragments in the vicinity of the Au cluster (Table 1). Figure 5 shows OPDOS plots of the 2CS8-Au and 2CSe8-Au complexes. The stronger interaction between fragments in 2CSe8-Au manifests

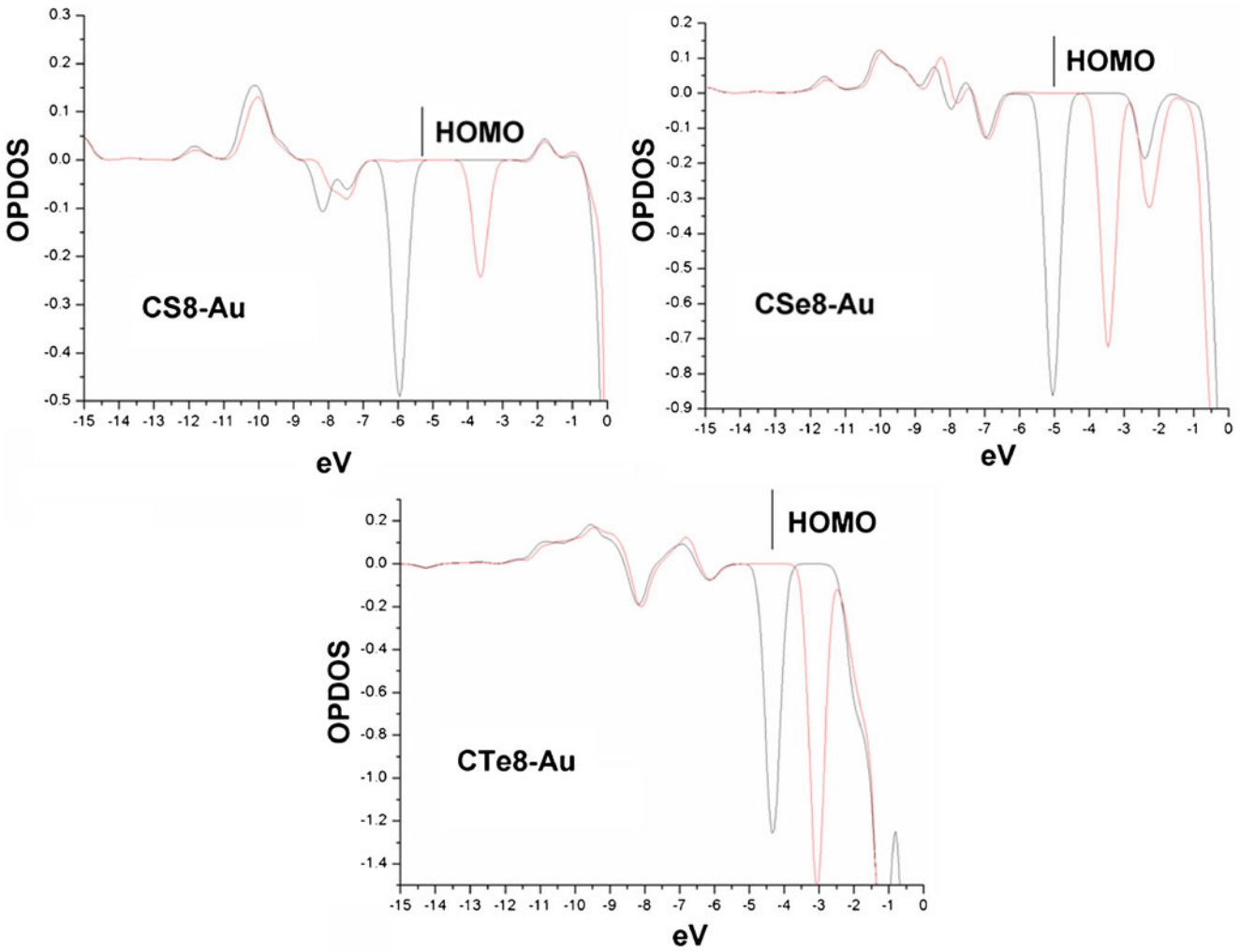

Fig 3 OPDOS plots of the alpha (*red*) and beta (*black*) levels of the CS8-Au, CSe8-Au, and CTe8-Au complexes

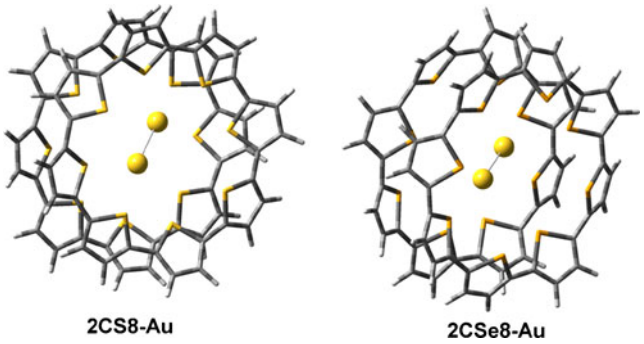

Fig. 4 Optimized geometries of the 2CS8-Au and 2CSe8-Au complexes

itself in the fact that the bonding levels in 2CSe8-Au have more bonding character than antibonding (more positive values of OPDOS). Although the antibonding levels at −7 and −6 eV are full in both complexes, in the case of 2CSe8-Au, the levels at around −6 eV show less antibonding character, and the bonding levels between −12 and −8 eV show more bonding character.

3CS8-Au and 3CSe8-Au

The geometries of these complexes are very similar (Fig. 6). The distance between the closest Au atoms is 2.64 Å for 3CS8-Au and 2.65 Å for 3CSe8-Au. The shortest heteroatom to Au atom distances are 2.75 and 2.77 Å, respectively. Both the absolute binding energies and the binding energies per atom are higher than those of the 2CS8-Au and 2CSe8-Au complexes (Table 2).

The same situation is noted for the natural charges, which are more negative. The binding energy and natural charge have higher absolute values for 3CSe8-Au. The negative charge on the Au_3 cluster reaches −1.23 *e*, while the binding energy shifts to 62.7 kcal mol^{-1}, revealing a relatively strong interaction between the Au_3 cluster and the nanoaggregate. OPDOS plots demonstrate (Fig. 7) that bonding levels in the region from −11 to −9 eV have more bonding character, and that the antibonding levels in the region from −8 to −5 eV have less antibonding character for 3CSe8-Au, thus explaining the higher interaction energy between the Au_3 cluster and the nanoaggregate for 3CSe8-Au.

4CS8-Au and 4CSe8-Au

Two different isomers (T and R) were detected for 4CS8-Au and 4CSe8-Au (Fig. 8). In the case of 4CS8-Au, the T isomer is slightly more stable (1.49 kcal mol^{-1}), while the R isomer is the lowest-energy structure for 4CSe8-Au, as it is 0.49 $kcalmol^{-1}$ more stable than the T isomer. Since this energy difference is rather small, all of these isomers can coexist provided the activation energy for the interconversion is low.

Table 2 shows the properties of these isomers. Since their total energies are very similar, their binding energies are also similar. Indeed, the natural charge on the Au cluster is almost identical for the two isomers as well. While the binding energy between the nanoaggregate and the Au cluster is increased compared to the corresponding trimer, the binding energy per atom is slightly lower than for the trimer. A similar situation is noted for the natural charge on an Au atom, as similar values are observed to those found for 3CS8-Au and 3CSe8-Au. The charge is more negative and the binding energy higher for Se than for S, in line with other cases. The geometry of the Au_4 cluster differs slightly between 4CS8-Au-R and 4CSe8-Au-R. The shortest distance between Au atoms in Au_4 is 2.69 Å

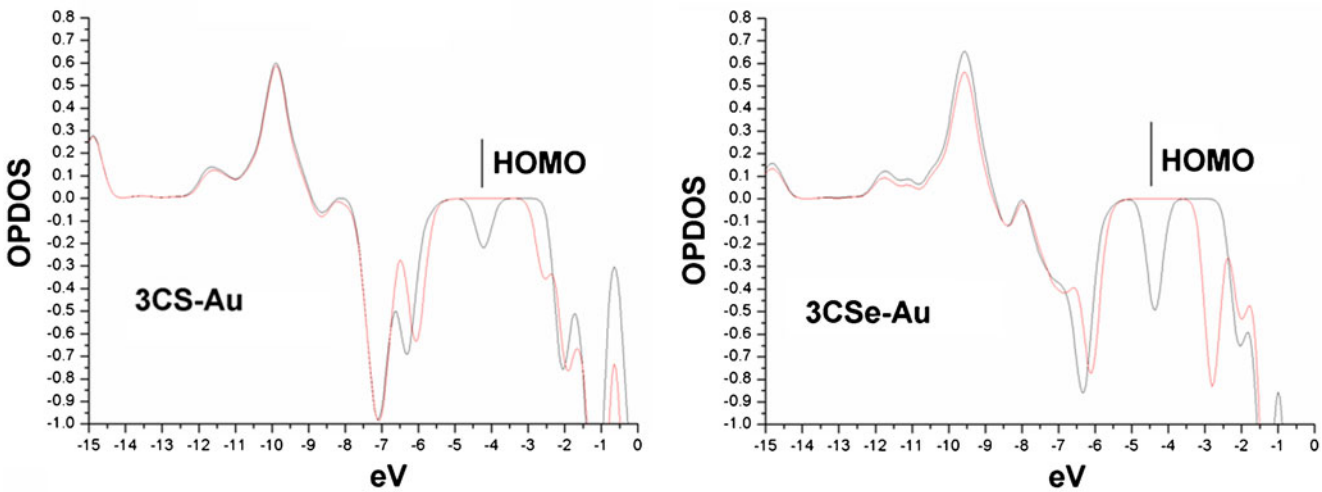

Fig. 5 OPDOS plots of the 2CS8-Au and 2CSe8-Au complexes

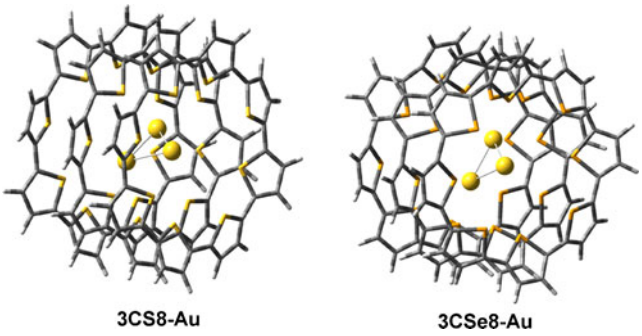

Fig. 6 Optimized geometries of the 3CS8-Au and 3CSe8-Au complexes

in 4CS8-Au-R and 2.73 Å in 4CSe8-Au-R. On the other hand, the gold clusters in 4CS8-Au-T and 4CSe8-Au-T are very much alike, and the difference in the distance between Au atoms does not exceed 0.01 Å. The shortest heteroatom to Au distance does, however, differ in 4CS8-Au-T and 4CSe8-Au-T due to the larger VDW radius of Se compared to that of S: it is 2.65 and 2.72 Å, respectively. Figure 9 shows OPDOS plots for all of the isomers of 4CS8-Au and 4CS8-Au. As seen, the OPDOS plots are very similar for occupied levels when comparing the R and T isomers of each nanoaggregate, but there are clear differences between the OPDOS plots for the corresponding isomers of 4CS8-Au and 4CSe8-Au. In the case of 4CSe8-Au, the bonding levels in the range between −12 and −9 eV are more binding in character than the corresponding levels for 4CSe8-Au. On the other hand, the antibonding levels between −8 and −6 eV are more antibonding in character for 4CS8-Au. This leads to the higher binding energy between the Au_4 cluster and the nanoaggregate in the case of 4CSe8-Au.

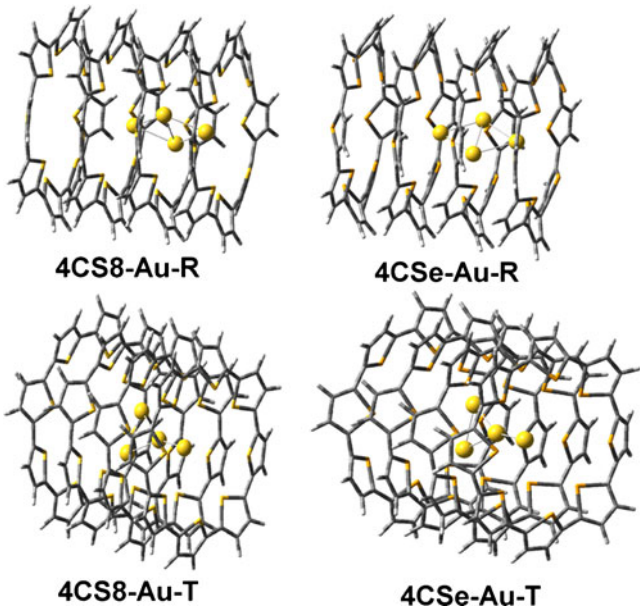

Fig. 8 Optimized geometries of the 4CS8-Au and 4CSe8-Au complexes

6CS8-Au and 6CSe8-Au

As also seen for 4CS8-Au and 4CSe8-Au, two different isomers were detected for 6CS8-Au and two for 6CSe8-Au: 6CS8-Au-T, 6CSe8-Au-T, 6CS8-Au-R, and 6CSe8-Au-R. The geometries of the R and T isomers are very similar (Fig. 10). The main difference between them is the shorter gold to heteroatom distance in 6CS8-Au, which is due to the smaller VDW radius of sulfur. The shortest Au–S distance in 6CS8-Au-T is 2.72 Å, whereas it is 2.75 Å in 6CSe8-Au-T. For the 6CS8-Au complex, the R isomer is 2.6 kcal mol^{-1} more stable than the T isomer, while for the 6CSe8-Au complex, the T isomer is 3.40 kcal mol^{-1} more stable than the R isomer.

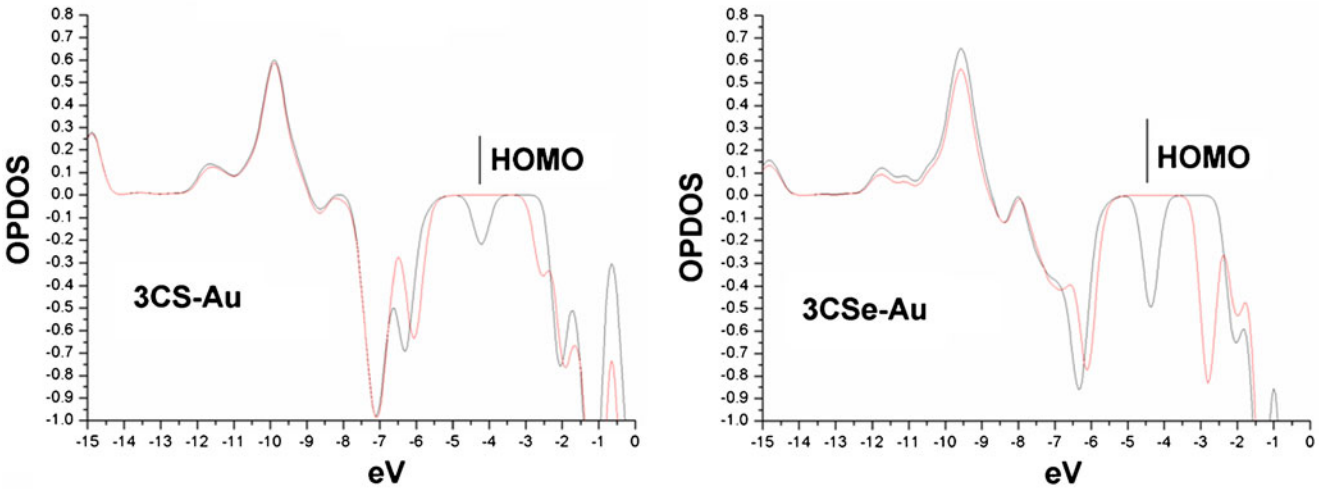

Fig. 7 OPDOS plots of the alpha (*red*) and beta (*black*) levels of the 3CS8-Au and 3CSe8-Au complexes

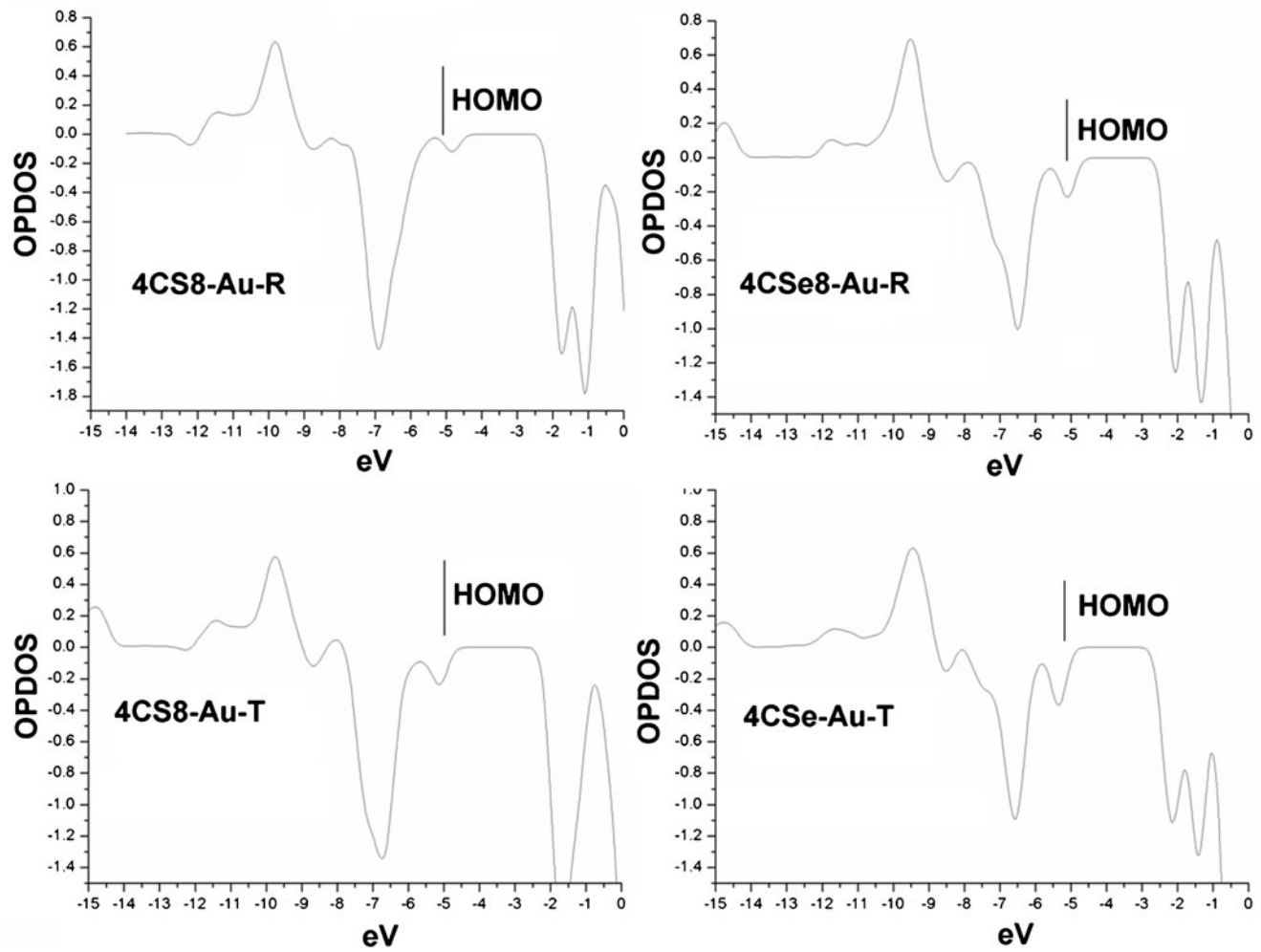

Fig. 9 OPDOS plots of the 4CS8-Au and 4CSe8-Au complexes

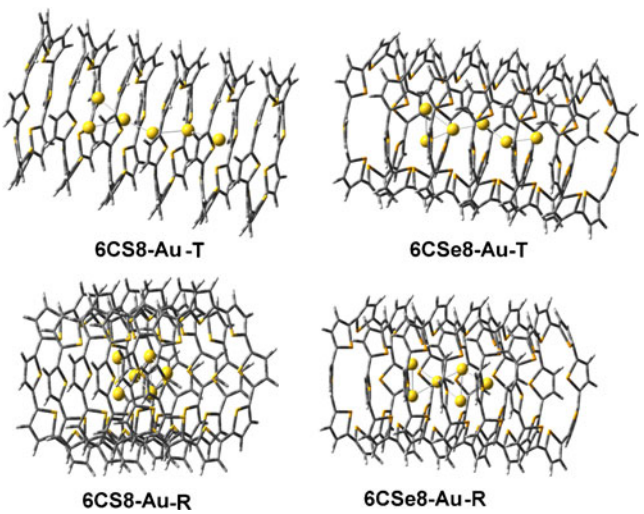

Fig. 10 Optimized geometries of the 6CS8-Au-T, 6CSe8-Au-T, 6CS8-Au-T-R, and 6CSe8-Au-R complexes

Unlike the other complexes, where the binding energy between the Au cluster and the nanoaggregate increases with the number of Au atoms, the binding energy between the Au_6 cluster and the nanoaggregate 6CS8 or 6CSe8 is less than that between the Au_4 cluster and 4CS8 or 4CSe8, respectively. As seen in Table 2, this decrease is similar for both systems: 14–15 kcal mol^{-1}. This decrease in binding energy is related to the geometry of the Au_6 cluster. For all of the other clusters, the geometry of the lowest-energy standalone Au cluster does not change when it is positioned inside the nanoaggregate. On the other hand, for the Au_6 cluster, the geometry changes upon insertion. The lowest-energy standalone isomer of Au_6 is a plane D_{3h} structure [35]. The largest distance between Au atoms in this cluster is more than 5 Å, making it larger than the internal diameters of the CS8 and CSe8 macrocycles, which are ~4 Å. Therefore, the six Au atoms form an extended structure

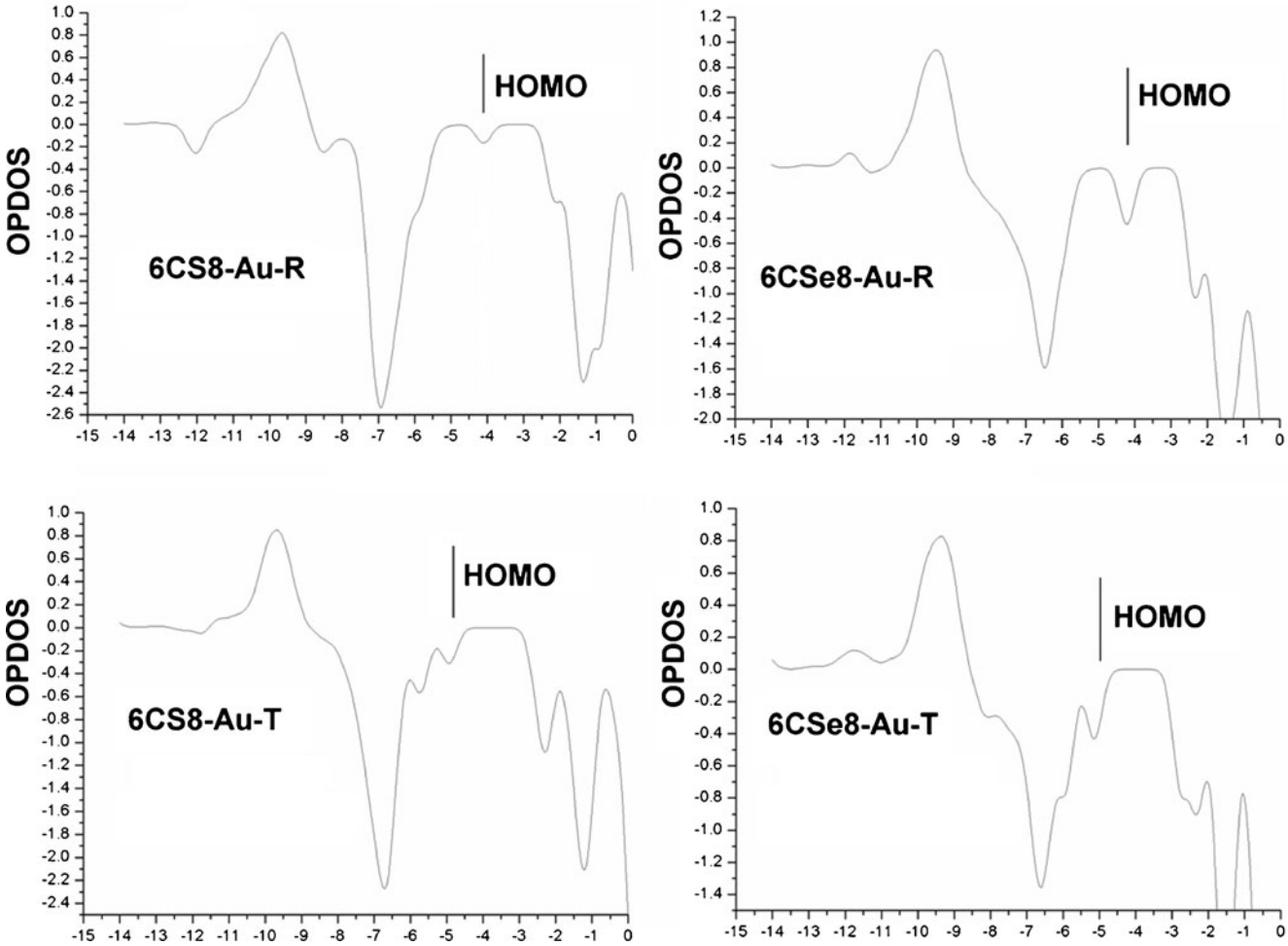

Fig. 11 OPDOS plots of the 6CS8-Au and 6CSe8-Au complexes

inside the nanoaggregate cavity. Since the lowest-energy structure of the gold cluster is used to calculate the binding energy, the reorganization energy (E_r) needed to change the Au_6 cluster geometry decreases the estimated binding energy. E_r can be calculated as the difference in electronic energy between the lowest-energy standalone isomer of Au_6 and the lowest-energy Au_6 cluster inside the nanoaggregate. The calculated E_r values for 6CS8-Au-T and 6CSe8-Au-T are 49.7 and 50.1 kcal mol^{-1}, respectively. Therefore, the binding energies for 6CS8-Au-T and 6CSe8-Au-T, without taking into account E_r, are 102.7 and 109.6 kcal mol^{-1}, respectively, or 17.1 and 18.3 kcal mol^{-1} per atom. These values are very close to those seen for other complexes. Therefore, the relatively low binding energies observed for 6CS8-Au and 6CSe8-Au are entirely due to E_r. However, the reorganization energy is significantly lower than the energy gained through the interactions of the gold cluster with the nanoaggregate, thus making the formation of the complex thermodynamically viable. The natural charge on the gold cluster reaches −1.90 *e* for 6CS8-Au-T and −2.60 *e* for 6CSe8-Au-T, which are similar in terms of the charge per Au atom to those seen for the other complexes and for 6CS8-Au-R and 6CSe8-Au-R. The OPDOS plots shown in Fig. 11 demonstrate that the higher binding energies obtained for 6CSe8-Au than for 6CS8-Au are due to decreased antibonding character of the levels between −8 and −5 eV in the case of 6CSe8-Au.

Conclusions

Among the three studied macrocycles, only CS8 and CSe8 are capable of nanoaggregate formation. Tellurophene fragments adopt the *anti* conformation in the lowest-energy structure of CTe8, thus impeding a tubular arrangement of the macrocycles. CS8 and CSe8 form stable nanoaggregates. Interestingly, nCSe8 nanoaggregates have slightly lower binding energies than nCS8 nanoaggregates due to less efficient conjugation in the former. The binding energies of the inclusion complexes for individual macrocycles increase from CS8-Au to CTe8-Te, and the lowest-energy conformations differ

among the three complexes. In the case of CS8-Au, the gold atom is positioned in the center of the cavity, while it is off-center in CSe8-Au and CTe8-Au. The binding energy between the nanoaggregate and the gold cluster is always higher for the nCSe8-Au nanoaggregate than for the corresponding (same n) nCS8-Au nanoaggregate, due to the higher affinity of Se for Au in such complexes. The interactions of the gold cluster with the nanoaggregate walls can change the geometry of the most stable isomer for the cluster. Thus, for 4CS8-Au, the most stable structure of Au_4 is T-shaped, while a rhombic structure (R) is the lowest-energy structure for standalone Au_4 and for 4CSe8-Au. The relative energies of the different isomers are rather similar, suggesting that they coexist. For 6CS8-Au and 6CSe8-Au, the geometry of the Au_6 cluster is different from that of the standalone Au_6 cluster due to the geometric restrictions imposed by the nanoaggregate cavity. The reorganization energy needed to change the geometry of the cluster decreases the binding energies of 6CS8-Au and 6CSe8-Au, making these binding energies lower than those of some smaller systems; however, the formation of a complex between Au_6 and a nanoaggregate with six CS8 or CSe8 macrocycles is still thermodynamically viable.

Acknowledgments The authors acknowledge financial support from Programa de Apoyo a Proyectos de Investigación e Innovación Tecnológica (PAPIIT) Mexico (grant IN-100712/23).

References

1. Coskun A, Spruell JM, Barin G, Dichtel WR, Flood AH, Botros YY, Stoddart JF (2012) High hopes: can molecular electronics realise its potential? Chem Soc Rev 41:4827–4859
2. Fabre B (2010) Ferrocene-terminated monolayers covalently bound to hydrogen-terminated silicon surfaces. Toward the development of charge storage and communication devices. Acc Chem Res 43:1509–1518
3. Dadosh T, Gordin Y, Krahne R, Khivrich I, Mahalu D, Frydman V, Sperling J, Yacoby A, Bar-Joseph I (2005) Measurement of the conductance of single conjugated molecules. Nature 436:677–680
4. Song H, Kim Y, Jang YH, Jeong H, Reed MA, Lee T (2009) Observation of molecular orbital gating. Nature 462:1039–1043
5. Tour JM (2000) Molecular electronics. Synthesis and testing of components. Acc Chem Res 33:791–804
6. Carroll RL, Gorman CB (2002) The genesis of molecular electronics. Angew Chem Int Ed 41:4378–4400
7. Seminario JM, Zacarias AG, Tour JM (2000) Theoretical study of a molecular resonant tunneling diode. J Am Chem Soc 122:3015–3020
8. Brandbyge M, Mozos J-L, Ordejón P, Taylor J, Stokbro K (2002) Density-functional method for nonequilibrium electron transport. Phys Rev B 65:165401
9. Soler JM, Artacho E, Gale JD, García A, Junquera J, Ordejón P, Sánchez-Portal D (2002) The SIESTA method for ab initio order-*N* materials simulation. J Phys Condens Matter 14:2745–2779
10. Taylor J, Guo H, Wang J (2001) Ab initio modeling of quantum transport properties of molecular electronic devices. Phys Rev B 63:245407
11. Kondo Y, Takayanagi K (2000) Synthesis and characterization of helical multi-shell gold nanowires. Science 289:606–608
12. Ajayan PM, Iijima S (1993) Capillarity-induced filling of carbon nanotubes. Nature 361:333–334
13. Grobert N, Hsu WK, Zhu YQ, Hare JP, Kroto HW, Walton DRM, Terrones M, Terrones H, Redlich P, Rühle M, Escudero R, Morales F (1999) Enhanced magnetic coercivities in Fe nanowires. Appl Phys Lett 75:3363–3365
14. Hsin YL, Hwang KC, Chen FR, Kai JJ (2001) Production and in situ metal filling of carbon nanotubes in water. Adv Mater 13:830–833
15. Hu J, Bando Y, Zhan J, Zhi C, Golberg D (2006) Carbon nanotubes as nanoreactors for fabrication of single-crystalline Mg_3N_2 nanowires. Nano Lett 6:1136–1140
16. Hirsch A, Vostrowsky O (2005) Functionalization of carbon nanotubes. Top Curr Chem 245:193–237
17. Burghard M (2005) Electronic and vibrational properties of chemically modified single-wall carbon nanotubes. Surf Sci Rep 58:1–109
18. Terrones H, Lopez-Urias F, Munoz-Sandoval E, Rodriguez-Manzo JA, Zamudio A, Elias AL, Terrones M (2006) Magnetism in Fe-based and carbon nanostructures: theory and applications. Solid State Sci 8:303–320
19. Ivanovskaya VV, Makurin YN, Ivanovskii AL (2005) Fullerene peapods and related nanomaterials: synthesis, structure and electronic structure. In: Diudea M (ed) Nanostructures: novel architectures. Nova Science, New York, pp 9–24
20. Guerret-Piécourt C, Le Bouar Y, Loiseau A, Pascard H (1994) Relation between metal electronic structure and morphology of metal compounds inside carbon nanotubes. Nature 372:761–765
21. Leonhardt A, Ritschel A, Kozhuharova R, Graff A, Mühl T, Huhle R, Mönch I, Elefant D, Schneider CM (2003) Synthesis and properties of filled carbon nanotubes. Diamond Relat Mater 12:790–793
22. Grobert N, Terrones M, Osborne AJ, Terrones H, Hsu WK, Trasobares S, Zhu YQ, Hare JP, Kroto HW, Walton RM (1998) Thermolysis of C60 thin films yields Ni-filled tapered nanotubes. Appl Phys A 67:595–598
23. Setlur AA, Lauerhaas JM, Dai JY, Chang RPH (1996) A method for synthesizing large quantities of carbon nanotubes and encapsulated copper nanowires. Appl Phys Lett 69:345–347
24. Loiseau A, Pascard H (1996) Synthesis of long carbon nanotubes filled with Se, S, Sb and Ge by the arc method. Chem Phys Lett 256:246–252
25. Flores P, Guadarrama P, Ramos E, Fomine S (2008) Tubular aggregates of cyclic oligothiophenes. A theoretical study. J Phys Chem A 112:996–4003
26. Fomine S (2012) Stabilization of gold and silver nanowires inside cyclo[8]thiophene nanoaggregates. A theoretical study. J Nanopart Res 14:979–990
27. Sugimoto R, Yoshino K, Inoue S, Tsukago K (1985) Preparation and property of polytellurophene and polyselenophene. Jap J Appl Phys 24:L425–L427
28. Salzner U, Lagowski JB, Pickup PG, Poirier RA (1998) Comparison of geometries and electronic structures of polyacetylene, polyborole, polycyclopentadiene, polypyrrole, polyfuran, polysilole, polyphosphole, polythiophene, polyselenophene, and polytellurophene. Synth Met 96:177–189
29. Patra A, Bendikov M (2010) Polyselenophenes. J Mater Chem 20:422–433
30. Fuhrmann G, Debaerdemaeker T, Bäuerle P (2003) C–C bond formation through oxidatively induced elimination of platinum complexes. A novel approach towards conjugated macrocycles. Chem Commun 8:948–949
31. Frisch MJ et al. (2009) Gaussian 09, revision B.01. Gaussian, Inc., Wallingford
32. Zhao Y, Truhlar DG (2008) The M06 suite of density functionals for main group thermochemistry, thermochemical kinetics, noncovalent interactions, excited states, and transition elements: two new

functionals and systematic testing of four M06-class functionals and 12 other functionals. Theor Chem Account 120:215–241
33. Yanai T, Tew D, Handy N (2004) A new hybrid exchange–correlation functional using the Coulomb-attenuating method (CAM-B3LYP). Chem Phys Lett 393:51–57
34. Baetzold RC (1971) Calculated properties of metal aggregates. I. Diatomic molecules. J. Chem Phys 55:4355–4363
35. Wang J, Wang G, Zhao J (2002) Density-functional study of Au_n(n=2–20) clusters: lowest-energy structures and electronic properties. Phys Rev B 66:035418
36. Fournier R (2001) Theoretical study of the structure of silver clusters. J Chem Phys 115:2165–2177
37. Gorelsky SI (2011) AOMix: program for molecular orbital analysis, version 6.5. http://www.sg-chem.net/
38. Gorelsky SI, Ghosh S, Solomon EI (2006) Mechanism of N_2O reduction by the μ_4-S tetranuclear Cu_Z cluster of nitrous oxide reductase. J Am Chem Soc 128:278–290
39. Zade SS, Bendikov M (2006) Cyclic oligotiophenes: novel organic materials and models for polythiophene. A theoretical study. J Org Chem 71:2972–2981